Assessing the potential of the Atmospheric Infrared Sounder (AIRS) surface temperature and specific humidity in turbulent heat flux estimates in the Southern Ocean

Shenfu Dong,[1] Sarah T. Gille,[2] Janet Sprintall,[2] and Eric J. Fetzer[3]

Received 28 May 2009; revised 13 November 2009; accepted 17 December 2009; published 13 May 2010.

[1] Surface air temperature (T_A), sea surface temperature (T_O), and surface specific humidity (q_a) satellite retrievals from the Atmospheric Infrared Sounder (AIRS) are compared with shipboard measurements across Drake Passage for the period from September 2002 to June 2007. The objective is to evaluate whether AIRS retrievals, in conjunction with microwave sea surface temperatures from the Advanced Microwave Scanning Radiometer (AMSRE), can provide sufficiently accurate parameters to estimate sensible and latent heat fluxes in the data-limited Southern Ocean. The collocated data show that both AIRS T_A and T_O are colder than those from shipboard measurements, with a time mean bias of −2.03°C for T_A and −0.22°C for T_O. Results show that air-sea temperature difference ($T_A - T_O$), q_a, and relative humidity (RH) are the major factors contributing to the differences between satellite and shipboard temperature measurements. Differences in AIRS and shipboard T_A (ΔT_A) decrease with increasing $T_A - T_O$, and ΔT_A increases with increasing RH, whereas differences in AIRS and shipboard T_O (ΔT_O) increase with both increasing $T_A - T_O$ and increasing q_a. The time mean q_a from AIRS is lower than the shipboard q_a by 0.69 g/kg. Statistical analyses suggest that $T_A - T_O$, cloud, and q_a are the major contributors to the q_a difference (Δq_a). Δq_a becomes more negative with increasing $T_A - T_O$ and increasing cloud fraction. Δq_a also becomes more negative as q_a increases. Compared with T_A, T_O, and $T_A - T_O$, from the National Centers for Environmental Prediction/National Center for Atmospheric Research Reanalysis (NCEP), AIRS-derived and AMSRE-derived variables show more small-scale spatial structure, as is also typical of the ship observations. Although AIRS q_a gives a better representation of the full range of values of shipboard q_a, its deviation from shipboard q_a is relatively large compared to NCEP q_a. Compared with several existing gridded flux products, turbulent fluxes estimated from AIRS and AMSRE data using bulk algorithms are better able to represent the full range of flux values estimated from shipboard parameters.

Citation: Dong, S., S. T. Gille, J. Sprintall, and E. J. Fetzer (2010), Assessing the potential of the Atmospheric Infrared Sounder (AIRS) surface temperature and specific humidity in turbulent heat flux estimates in the Southern Ocean, *J. Geophys. Res.*, *115*, C05013, doi:10.1029/2009JC005542.

1. Introduction

[2] Heat exchange between the atmosphere and the ocean is an important process in the climate system and reflects the interaction of the coupled climate system [e.g., *Barsguli and Battisti*, 1998; *Ciasto and Thompson*, 2008]. Global air-sea heat fluxes have been used in numerous aspects of climate studies over many time scales [*Taylor*, 2000; *Curry et al.*, 2004] and are needed to evaluate coupled atmosphere-ocean models and weather forecasting models. Thus, accurate estimates of air-sea heat fluxes are important, particularly in high latitudes, where air-sea exchanges play a key role in deepwater formation, which, in turn, is related to the meridional overturning circulation [e.g., *Kuhlbrodt et al.*, 2007]. However, commonly used surface flux estimates from the National Centers for Environmental Prediction/National Center for Atmospheric Research Reanalysis (NCEP) and the European Centre for Medium-Range Weather Forecasts Reanalysis 40 can differ by 100 W/m^2 or more on any given day, compared with typical daily values of 150–250 W/m^2 [*Dong et al.*, 2007]. An assessment of the upper ocean heat balance in the Southern Ocean [*Dong et*

[1]Cooperative Institute for Marine and Atmospheric Studies, Rosenstiel School of Marine and Atmospheric Science, University of Miami, Miami, Florida, USA.
[2]Scripps Institution of Oceanography, University of California, San Diego, California, USA.
[3]Jet Propulsion Laboratory, Pasadena, California, USA.

0148-0227/10/2009JC005542

al., 2007] suggested that air-sea heat flux is the largest contributor to errors in the heat balance. A better air-sea heat flux product is needed to improve our understanding of upper ocean processes related to the meridional overturning circulation.

[3] The net air-sea heat flux includes four components: shortwave radiation, longwave radiation, sensible heat flux, and latent heat flux. Standard bulk flux formulas for the sensible (SH) and latent (LH) heat components depend on air-sea temperature difference, specific humidity, and wind speed at the sea surface [e.g., *Smith*, 1988; *Fairall et al.*, 1996],

$$\mathrm{SH} = \rho_a C_e C_p W (T_A - T_O) \tag{1}$$

$$\mathrm{LH} = \rho_a C_e L_e W (q_s - q_a), \tag{2}$$

where ρ_a is air density, C_e is the exchange coefficient, C_p is heat capacity, and W is near-surface wind speed relative to a stationary ocean. T_O and T_A are surface ocean and air temperature, respectively. L_e is latent heat of vaporization, and q_s and q_a are saturated specific humidity at the temperature of the ocean surface and the specific humidity of the air above it, respectively.

[4] It is impractical to make in situ measurements of these parameters with sufficiently high spatial and temporal resolution to estimate the global heat flux for climate studies. Satellite measurements for sea surface temperature (T_O) and wind speed have been readily available since the late 1980s, providing a relatively long time series of these climate variables to compute latent and sensible heat fluxes at global scales [*Bentamy et al.*, 2003; *Curry et al.*, 2004, *Singh et al.*, 2005; *Tomita and Kubota*, 2006]. Satellite retrievals of near-surface air temperature and humidity have proven difficult, although a set of sensors aboard the NASA Earth Observing System (EOS) Aqua satellite offer new possibilities for measuring these quantities. *Jackson et al.* [2006] assessed the possibility of combining microwave measurements from the Advanced Microwave Sounding Unit-A with other microwave satellite sensors to retrieve near-surface air temperature and humidity. Here, we examine the potential for improving surface flux estimates by using observations from the Aqua Atmospheric Infrared Sounder (AIRS), which provides three-dimensional maps of air, water, and cloud properties, with the potential to obtain higher spatial resolution than is possible with microwave sensors. We will use AIRS observations in combination with all-weather T_O from the Advanced Microwave Scanning Radiometer (AMSRE), also on board Aqua, to estimate sensible and latent heat fluxes in the Drake Passage.

[5] The goal of AIRS is to provide more accurate information on the vertical profiles of atmospheric temperature and moisture for climate research and weather forecasting. *Divakarla et al.* [2006] suggested that temperature and water vapor profiles from AIRS are in very good agreement with those from radiosonde observations, which were collocated within 1 h temporal separation and 200 km spatial separation. Although the atmospheric boundary layer is not the focus of the AIRS measurements, near-surface parameters are either provided directly in AIRS products or can be extracted from the vertical profiles. The near-surface parameters that AIRS measures, such as air temperature and specific humidity, are required by the bulk formulas that estimate air-sea heat fluxes (i.e., equations (1) and (2)). However, validation for the AIRS measurements has been done mainly in the nonpolar regions [*Fetzer*, 2006], and high-latitude conditions are not yet well represented in the AIRS validation/calibration process. *Susskind et al.* [2006] found a small degradation of AIRS retrieval accuracy with increasing cloud cover, and high-latitude regions such as the Southern Ocean can experience particularly frequent cloud cover. Thus, it is important to first validate AIRS retrievals in the Southern Ocean to determine their potential for calculating sensible and latent heat fluxes. Recently, relative humidity from the AIRS measurements over Antarctica has been validated using radiosonde observations [*Gettelman et al.*, 2006], although the radiosondes in that study were over ice, where the atmospheric boundary layer may behave differently than it does over the open ocean.

[6] In this study we present one of the first attempts to evaluate the performance of the AIRS surface air temperature (T_A), sea surface temperature (T_O), and specific humidity (q_a) in the Southern Ocean. Our focus on the Southern Ocean contrasts with the bulk of satellite calibration and validation studies, which have for the most part made use of buoy and ship observations primarily from the tropics and subtropics [e.g., *Mears et al.*, 2001; *Barton et al.*, 2004; *Gentemann et al.*, 2004]. Our ultimate goal is to determine whether they are accurate enough to use in sensible and latent heat flux estimations. The Antarctic research vessel and supply ship *Laurence M. Gould* of the U.S. Antarctic Program provides measurements of surface atmospheric parameters to evaluate the accuracy of AIRS surface measurements in the Drake Passage. The data sets used in this study and the process of collocating the various data sets are described in section 2. In section 3 we compare AIRS near-surface temperature retrievals with shipboard measurements and discuss possible causes for their differences. Our results show that both air-sea temperature difference ($T_A - T_O$) and specific humidity (q_a) affect the near-surface temperature differences between satellite retrievals and shipboard measurements. Comparison of surface q_a from AIRS retrieval and shipboard measurements and possible causes for their differences are discussed in section 4. The seasonal and cross-passage variations in near-surface temperature and specific humidity differences between AIRS and shipboard measurements are given in section 5. In section 6, we examine the potential uncertainties in the derived turbulent latent and sensible heat fluxes that use the AIRS near-surface retrievals. Finally, we present a discussion and summary in section 7.

2. Data Description and Processing

2.1. Data Description

2.1.1. Atmospheric Infrared Sounder (AIRS) Data

[7] AIRS is one of six instruments on board the EOS Aqua satellite, representing the most advanced atmospheric sounding system ever deployed in space. The Aqua satellite, launched in May 2002, follows a Sun-synchronous polar orbit, so observations occur at roughly the same local time each day. Although the observational times of AIRS are not exactly fixed due to precession and changes in the sampling

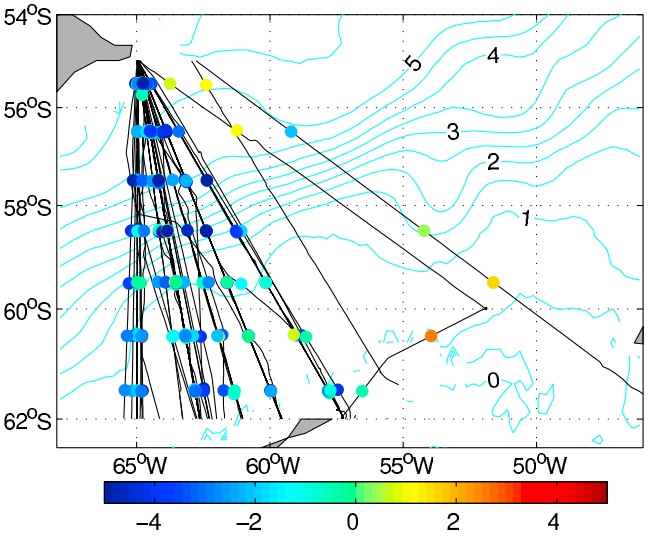

Figure 1. Repeat R/V *Laurence M. Gould* crossings (black lines) in the Drake Passage between September 2002 and June 2007. The colored dots indicate the mean near-surface air temperature difference between Atmospheric Infrared Sounder (AIRS) and shipboard measurements at collocated locations. Contours indicate mean sea surface temperature from Advanced Microwave Scanning Radiometer (AMSRE). Units are °C.

location across the scan, in general the orbit moves northward at 1330 and southward at 0130 at equator local time and crossings at 55°S are around 1500 and 0100 local time. In the Drake Passage (55°S–62°S) the daily observational time varies within a 2 h window. AIRS is a cross-track scanning, high-spectral resolution infrared sounder, which is able to retrieve an entire profile of temperature and water vapor in the presence of up to 70% cloud cover [*Aumann et al.*, 2003]. In this study we evaluate the version 5 daily level 3 (L3) near-surface products [*Susskind et al.*, 2003]. The AIRS L3 products are derived from L2 (satellite swath) data that have been binned and averaged onto a 1° × 1° grid. For this study, we use surface T_A at 2 m above sea level and T_O directly from the AIRS L3 products, and we determine surface q_a from the base of the vertical profile of AIRS q_a data, as discussed in section 2.2. The data have been validated for nonpolar latitudes (50°S–50°N), but few high-latitude observations are available to provide validation in polar conditions. We validate AIRS surface parameters (T_A, T_O, and q_a) in the Drake Passage over a nearly 5 year period from September 2002 (the start time of the AIRS data) through June 2007. In nonpolar regions, the estimated uncertainties in AIRS near-surface variables are relatively large: the uncertainty for both AIRS T_A and T_O is 1 K [*Aumann et al.*, 2006], and for q_a it is 15%–25% of q_a [*Tobin et al.*, 2006].

[8] The bulk formula for sensible heat flux (equation (1)) depends on the air-sea temperature difference ($T_A - T_O$), not on T_A or T_O alone. Although AIRS provides T_O, the infrared measurements are still strongly influenced by water vapor and cloud [e.g., *Merchant and Harris*, 1999; *Vazquez-Cuervo et al.*, 2004]. For AIRS products, the error estimates are generated for T_A and T_O independently although using the same methodology. Error thresholds are applied that are stricter for T_O than for T_A. This can result in observation times when T_O are masked out, mostly due to cloud effects, but T_A is provided (E. T. Olson, personal communication, 2010). In our Drake Passage study area, AIRS T_O is unavailable ~60% of the total time period. In contrast to infrared radiation, microwave radiation is capable of penetrating through cloud, which is particularly useful in the perpetually cloudy Southern Ocean. Thus, in addition to evaluating the AIRS retrievals, here we also evaluate T_O from AMSRE, a multichannel passive microwave radiometer on board the same Aqua satellite [*Wentz and Meissner*, 2000, 2007]. A comparison of the availability of the AIRS T_O with the availability of the AMSRE T_O suggested that 80% of the AIRS gaps were due to the presence of clouds. The daily version 5 AMSRE T_O are on a 0.25° longitude by 0.25° latitude grid. In previous work, *Dong et al.* [2006a] found that, in comparison with infrared measurements, AMSRE provides T_O measurements with little bias relative to in situ observations in the Southern Ocean. Finally, we compare Drake Passage shipboard measurements of $T_A - T_O$ with the satellite $T_A - T_O$ derived using T_A from AIRS and T_O, either from AIRS or from AMSRE, and we ask specifically whether these are sufficiently accurate to be useful for sensible heat flux estimates.

2.1.2. Shipboard Measurement

[9] To date, the deployment of large surface meteorological buoys has been prevented in the Southern Ocean because of the frequency of severe weather conditions. For the same reason, there is relatively little ship traffic in the Southern Ocean. However, in 2002, new highly accurate meteorological and underway seawater intake systems were installed on the R/V *Laurence M. Gould* (LMG), the principal supply ship of the U.S. Antarctic Program for Palmer Station. The LMG crosses the Drake Passage approximately 20 times per year, providing year-round measurements for determination of the air-sea fluxes in the region. The T_A, relative humidity (RH), and pressure are measured at 10 m above sea level, and T_O is measured by a hull-mounted thermosalinograph (TSG) at 4 m below sea level. To compare with AIRS q_a, we calculated the shipboard q_a as the saturated humidity multiplied by the RH, where the saturated humidity is computed as a function of the shipboard T_A and pressure. As discussed in section 2.2, these measurements were adjusted slightly to represent the same heights as the AIRS retrievals. The 1 s raw data are averaged to 5 min sampling intervals. The meteorological instrumentation and TSG are generally calibrated on an annual basis. The calibration error specified by the TSG manufacturer is 0.01°C. However, *Dong et al.* [2006a] suggested that TSG measurements are 0.15°C warmer than measurements from high-resolution expendable bathythermographs in the Drake Passage region. The manufacturer's reported accuracies for T_A, RH, and atmospheric pressure from the shipboard automated meteorological system are 0.1°C, 1%, and 0.5 hPa, respectively, which implies a q_a accuracy of 0.07 g/kg. A total of 88 LMG crossings were completed over the concurrent period of the AIRS measurements, from September 2002 to June 2007 (Figure 1).

[10] In addition to evaluating AIRS retrievals, we are also interested in the performance of AIRS surface parameters relative to the NCEP products that have been widely used in

estimating air-sea heat fluxes [e.g., *Yu and Weller*, 2007]. *Dong et al.* [2007] suggested that, compared to available air-sea heat flux products, the NCEP variables provided the best air-sea heat flux estimates to close the heat budget in the Southern Ocean at the time of the study. Here we compare T_O and T_A at 2 m above sea level and surface q_a from NCEP with shipboard measurements from the LMG. This comparison will show how well the NCEP products in the Southern Ocean capture the variability of shipboard observations and will assess whether the AIRS products provide parameters that may lead to better estimates of latent and sensible heat fluxes. NCEP products have better temporal resolution (6 h) but coarser spatial resolution (1.88° in latitude and longitude) than AIRS L3 products. Thus, we would not expect that the NCEP data capture the strong frontal structure that is characteristic of the Antarctic Circumpolar Current [*Dong et al.*, 2006b].

2.1.3. Surface Turbulent Heat Fluxes

[11] A number of other turbulent heat flux products have been developed recently using satellite measurements, including three global products that are available during the first few years of our study period. Objectively analyzed air-sea heat fluxes (OAFlux) [*Yu and Weller*, 2007] are constructed through a combination of satellite observations, surface moorings, ship reports, and atmospheric model reanalyzed surface meteorology. Daily OAFlux products are available on a 1° grid for the period 1985–2006. Turbulent heat fluxes from the Japanese Ocean Flux data sets with Use of Remote sensing Observations version 2 (J-OFURO2) [*Kubota and Tomita*, 2007] are estimated mainly using satellite measurements, except T_A, which is from NCEP. The J-OFURO2 fluxes are also available on a 1° spatial resolution and one-day temporal resolution from 1988 to 2005. The Hamburg ocean atmosphere parameters and fluxes from satellite data (HOAPS-3) [*Andersson et al.*, 2007] provide satellite-derived turbulent heat fluxes with a 1° spatial grid and twice-daily temporal resolution covering the period July 1987 to 2005. The air temperature used in HOAPS-3 for the derivation of sensible heat flux is estimated from near-surface specific humidity and T_O. All three flux products are derived using the Coupled Ocean-Atmospheric Response Experiment bulk flux algorithm (COARE) [*Fairall et al.*, 2003]. COARE version 2.6 is used for HOAPS-3, whereas version 3.0 (COARE3.0) is used for OAFlux and J-OFURO2.

[12] In section 6 we will make flux estimates using shipboard measurements, AIRS retrievals, and NCEP variables from the COARE3.0 bulk formula. These flux estimates from AIRS and NCEP variables and those from OAFlux, J-OFURO2, and HOAPS-3 will be compared with the flux estimates from shipboard measurements to evaluate the potential of the AIRS surface retrievals in estimating turbulent heat fluxes.

[13] Scatterometers have been providing accurate global wind fields for a broad range of applications since the 1970s. Wind speeds from ocean scatterometers are a main data source for estimating global turbulent heat fluxes, such as OAFlux, J-OFURO2, and HOAPS-3. In this study, we use wind speed from the Center for Ocean-Atmospheric Prediction Studies (COAPS) in conjunction with AIRS/AMSRE parameters to estimate the turbulent heat fluxes, which will be compared with existing flux products to examine the possibility for flux improvement in the Southern Ocean. The COAPS gridded wind fields are objectively mapped onto a 1° × 1° grid from QuickSCAT scatterometer measurements and are available at 6 h temporal resolution [*Pegion et al.*, 2000].

2.2. Data Collocation

[14] To compare AIRS/AMSRE retrievals and NCEP data with shipboard measurements, we need to collocate all data to the same space and time grids. The collocation is done in three steps.

[15] 1. First, the 10 m shipboard measurements are adjusted to the same vertical level used in the AIRS and NCEP data. The shipboard T_A is adjusted to 2 m and pressure measured to sea level. The dry adiabatic lapse rate γ ($\gamma = -dT_A/dz = 9.8$°C/km) is used to convert T_A from 10 to 2 m. This is equivalent to adding a constant of only 0.076°C to all shipboard T_A measurements, and thus the choice of the lapse rate does not influence our results. To convert the 10 m pressure to surface pressure, we added a constant pressure adjustment of 1.2 hPa to the shipboard pressure measurements. The shipboard TSG measures ocean temperature at 4 m depth, while satellites detect the very top of the ocean surface. Infrared and microwave radiometers measure temperature at slightly different depths at the ocean surface. An infrared radiometer measures skin temperature at a depth of order 0.01 mm depending on the wavelength of the measurement, whereas a microwave radiometer measures the subskin temperature at a depth of approximately 1 mm. In addition, the AMSRE microwave sea surface temperature (SST) product from Remote Sensing Systems (RSS) was calibrated to match the Reynolds SST [*Wentz and Meissner*, 2007], that is, the "bulk" SST defined at a depth of ~1–5 m. *Dong et al.* [2006a] found that in the Southern Ocean, T_O values from AMSRE show good agreement with in situ T_O measurements. Hence here we will make no depth adjustments among the various T_O values.

[16] 2. Second, the high-resolution along-track shipboard measurements are averaged in 1° latitude bands to match the seven AIRS latitudinal grid points spanning Drake Passage (Figure 1). The 5 min calibrated underway shipboard data have an equivalent spatial resolution of ~0.014° latitude, and the ship requires about 6 h to travel 1° latitude. To assess the impact of the ship travel time, we explored differences in the averages obtained for various time spans, ranging from 1 to 6 h. Neither the averages themselves nor the analyses of in situ versus satellite measurements differ significantly as averaging times are varied. Therefore, following *Dong et al.* [2006a], we required that all the available shipboard data that are averaged to each 1° latitude grid point have a ±2.5 h time separation from each other and a ±0.5° latitude separation. The center point for both the time and latitude separations is at the center of the 1° latitude band. At the seven latitudinal grid points in Drake Passage, a total of 594 data points are generated through this averaging process.

[17] 3. The longitude and time of the data resulting from the latitudinal averaging process in step 2 differ from the AIRS regular 1° longitude grid and observational time. Therefore, the final step is to collocate the satellite data to the same longitude and time as the shipboard data. We extracted all the available AIRS day and night T_A, T_O, and

q_a and AMSRE T_O data at the same date and latitude as the 594 shipboard observations. Those AIRS data within a ±1° longitude band of the shipboard data are then linearly interpolated to the longitude of the averaged shipboard measurements (Figure 1). *Dong et al.* [2006a] suggested that the T_O diurnal cycle affects the temperature difference between satellite and in situ measurements due to the time separation. However, the T_O difference is not significant for time separations of less than 5 h in the Drake Passage, as the diurnal effect is small due to the relatively strong winds in the Southern Ocean [*Dong et al.*, 2006a]. Therefore, for consistency we use only satellite data collected within ±2.5 h of the available shipboard measurements. As in the work of *Dong et al.* [2006a], we found no significant differences in the comparison among AMSRE, AIRS, and shipboard temperature measurements for time separations of less than 5 h, and for q_a measurements there were no significant differences for time separations less than 1 day (not shown).

[18] Unfortunately, as noted above, because of clouds and gaps between satellite tracks, collocated surface T_A and T_O are not always available in the AIRS daily product. As a result, a total of 315 T_A (137 daytime and 178 nighttime) out of the possible 594 collocated data points are available. The availability of AIRS T_O is even lower than that of T_A, with a total of 181 T_O pairs (89 daytime and 92 nighttime) available. Thus, of the 88 LMG crossings, 26 crossings had five or more collocated AIRS T_A data available at the seven latitudinal grid points in Drake Passage (Figure 1), and only 7 crossings had five or more collocated AIRS T_O data.

[19] AIRS q_a is given at 12 standard pressure layers, with bottom boundaries ranging from 1000 to 100 hPa. We tested two methods for determining surface q_a from its vertical profile. In method 1, we assumed the surface boundary layer to be well mixed and used q_a from the lowest standard pressure layer. In method 2, we extrapolated q_a to the surface based on the assumption that q_a varies exponentially with pressure, using the estimates for layers centered at 962.5 hPa (925–1000 hPa) and 887.5 hPa (850–925 hPa). The two methods yield results with similar statistical relationships to the shipboard q_a and similar potential causes for the biases. However, method 1 showed a more negative mean bias of −1.09 g/kg compared to the mean bias of −0.69 g/kg from method 2. Thus, in this study we adopted method 2. Like surface temperatures, q_a is not always available in the AIRS daily product because of clouds and gaps between satellite tracks. Out of a total of 594 data points for which we sought q_a from AIRS, 315 (137 daytime and 178 nighttime) collocated values are extracted from AIRS within ±2.5 h of the shipboard measurements. Of the 88 LMG crossings, 30% had five or more grid points of collocated AIRS q_a data available for comparison to the shipboard data.

[20] To collocate the 0.25° AMSRE T_O with shipboard measurements, we averaged the same-day AMSRE T_O within ±0.5° latitude and ±0.5° longitude of the averaged shipboard grid point. As with the AIRS data, we used only AMSRE data collected within ±2.5 h of the shipboard measurements. This resulted in a total of 461 (203 daytime and 258 nighttime) collocated T_O from the cloud-penetrating microwave AMSRE measurements for comparison with the 594 available shipboard measurements. Over 70% of the Drake Passage crossings had five or more collocated grid point AMSRE T_O data available.

[21] The collocation of the coarser-resolution 1.88° Gaussian gridded NCEP data and the averaged shipboard measurements was relatively straightforward: we simply interpolated the 6-hourly NCEP data to the 594 averaged shipboard data locations and times.

[22] The collocated data pairs are not evenly distributed in all seasons. However, for all collocated parameters, their seasonal distributions are similar, with about 25% of the data in austral summer (January–March), 35% in autumn (April–June), 10% in winter (July–September), and 30% in spring (October–December). This seasonal distribution is due to the seasonal bias in shipboard observations. The shipboard measurements in the Drake Passage for conditions when AIRS are available show no significant difference from those when AIRS are not available during our study period (2002–2007), suggesting that AIRS gives a representative sampling of the near-surface parameters in our study region.

[23] Figure 2 shows an example of the collocated shipboard and satellite measurements for an October 2005 LMG Drake Passage crossing when satellite retrievals were mostly available. Spatial structures shown in the 5 min shipboard measurements (black lines) of all parameters and their 1° latitude averages (red lines) are very similar. Also shown in Figure 2 are the collocated AIRS/AMSRE (green/cyan lines) and NCEP (blue lines) data. The NCEP data are consistently too smooth to capture the observed variability. AIRS T_A (Figure 2a) and T_O (Figure 2b) are consistently colder than the corresponding shipboard measurements. However, compared with the NCEP data, the AIRS retrievals generally better represent the observed meridional variability. The exception is the AIRS q_a, which for this particular cruise does not demonstrate good agreement with the shipboard q_a (Figure 2d).

3. Evaluation of AIRS Surface Temperature

3.1. Evaluation of Surface T_A and T_O

[24] In order to evaluate the agreement between satellite and shipboard temperature measurements, we use statistical analyses of correlation and robust linear regression. Unless specified, we regress satellite parameters to the corresponding shipboard measurements, $X_{\mathrm{sat}} = a + bX_{\mathrm{ship}}$, where X_{sat} and X_{ship} represent satellite and shipboard measurements, respectively, and a and b are regression coefficients. If the regression slope b equals one, then satellite and shipboard measurements simply differ by the constant a. The statistical significance of the regression is tested using the value of the null correlation at 95% significance level.

[25] Table 1 summarizes the mean difference, root-mean-square (RMS) error, and standard error of T_A, T_O, $(T_A - T_O)$, and q_a between the satellite and shipboard measurements for the daytime, nighttime, and combined data sets. The AIRS T_A retrievals have an overall average cold bias of −2.03°C (Table 1). The difference between daytime and nighttime is marginal, with a slightly larger cold bias of −2.23°C during the daytime compared with the cold bias of −1.88°C during the nighttime (Table 1). Despite the large cold bias, a linear regression of AIRS T_A to shipboard T_A measurements (Figure 3a) shows that the air temperature scatters along a

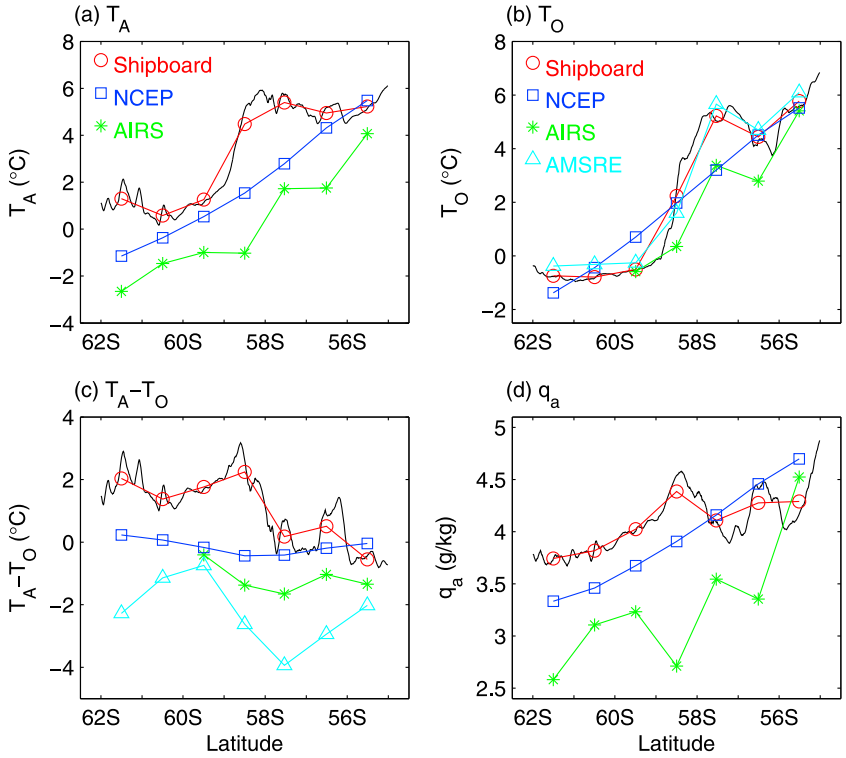

Figure 2. The collocated (a) surface air temperature, (b) sea surface temperature, (c) air-sea temperature difference, and (d) specific humidity for a Drake Passage crossing during October 2005. The black lines are the 5 min calibrated shipboard measurements, and the red circles are the corresponding 1° latitude averages. The squares and stars are collocated National Centers for Environmental Prediction (NCEP) and AIRS data, respectively. The triangles in Figures 2b and 2c are the T_O from AMSRE and ($T_A - T_O$) derived from AIRS T_A and AMSRE T_O.

line nearly parallel to the zero-bias line (also known as the 1:1 line), with a regression slope $b = 0.94$. This suggests that the biases in AIRS T_A are largely consistent with a constant offset of $a = 1.8$°C.

[26] Figure 3b shows that the shipboard T_O and the AMSRE T_O are highly correlated, with a correlation of 0.97, and they scatter closely along the zero-bias line. The nighttime T_O from AMSRE is colder than the shipboard value by −0.17°C, whereas during the daytime, AMSRE is warmer than the shipboard value by 0.01°C (Table 1). These results imply that, although the AMSRE SST was set to match the "bulk" SST and the strong wind reduces the diurnal effect in the Southern Ocean, the thermal skin effect of the surface ocean is still a concern. Thus a cool skin correction is applied to the LMG in situ measurements in computing the turbulent heat fluxes (section 6). Like AIRS T_A, AIRS T_O also has a cold bias compared with shipboard measurements, although there is no significant difference in the cold bias during daytime and nighttime (Table 1). The scatterplot of AIRS T_O versus shipboard T_O values (Figure 3c) shows relatively large deviations from the zero-bias line, suggesting that, in addition to being limited to cloud-free conditions, the AIRS T_O retrieval may also be affected by factors such as the stability of the atmospheric boundary layer.

[27] The bulk formula for sensible heat flux (equation (1)) depends on the air-sea temperature difference, ($T_A - T_O$). Regardless of the mean cold biases in AIRS T_A and T_O, Figures 3a and 3c show that both T_A and T_O scatter along lines parallel to the zero-bias line. However, in scatterplots comparing shipboard ($T_A - T_O$) with satellite observations, we see substantial deviation from the zero-bias line, regardless of whether we use the AIRS measurements alone (denoted $(T_A - T_O)_{\text{airs}}$) or AIRS T_A and AMSRE T_O (denoted $(T_A - T_O)_{\text{AMSRE}}$). Results are generally better using AMSRE T_O, which has a correlation coefficient of 0.57 versus 0.42 for AIRS data alone. On average, the satellite-derived ($T_A - T_O$) is more negative than shipboard measurements by −1.76°C for $(T_A - T_O)_{\text{AMSRE}}$ and by −1.25°C for $(T_A - T_O)_{\text{AIRS}}$, with most of this bias contributed by the cold bias in AIRS T_A (Table 1). With a 10 m/s wind speed, the cold bias of −1.76°C for $(T_A - T_O)_{\text{AMSRE}}$ would give an anomalous sensible heat loss to the atmosphere of 26 W/m^2.

[28] Scatterplots of NCEP parameters against shipboard measurements show that both T_A (Figure 4a) and T_O (Figure 4b) from NCEP compare well with in situ measurements, although NCEP has a cold bias of −0.30°C for T_A and a cold bias of −0.05°C for T_O (Table 1). The regression slopes (Figure 4) for both T_A and T_O are slightly lower than those from the AIRS regression analyses (Figure 3), whereas the correlations are slightly higher. Although NCEP T_A and T_O agree well with shipboard measurements, their difference $(T_A - T_O)_{\text{NCEP}}$ does not agree as well (Figure 4c), much as found for $(T_A - T_O)_{\text{AIRS}}$. As shown in Figure 4c, the scatter of $(T_A - T_O)_{\text{NCEP}}$ versus $(T_A - T_O)_{\text{ship}}$ deviates from the zero-bias line. This deviation can be attributed to the lower

Table 1. Temporal Mean Difference ± Standard Error, Root-Mean-Square Error, and Number of Collocated Data From Satellite and National Centers for Environmental Prediction With R/V *Laurence M. Gould* Shipboard Measurements of Near-Surface Air Temperature, Sea Surface Temperature, and Specific Humidity[a]

	Ascending (Daytime)		Descending (Nighttime)		All Data	
	Number of Data	Mean Difference	Number of Data	Mean Difference	Number of Data	Mean Difference
T_A (°C)						
AIRS	137	−2.23 ± 0.16(1.83)	178	−1.88 ± 0.14 (1.85)	315	−2.03 ± 0.10 (1.85)
NCEP					594	−0.30 ± 0.05 (1.18)
T_O (°C)						
AIRS	89	−0.16 ± 0.13 (1.22)	92	−0.27 ± 0.15 (1.40)	181	−0.22 ± 0.10 (1.31)
AMSRE	203	0.01 ± 0.05 (0.66)	258	−0.17 ± 0.04 (0.63)	461	−0.09 ± 0.03 (0.64)
NCEP					579	−0.05 ± 0.04 (0.84)
$T_A - T_O$ (°C)						
AIRS only	76	−1.63 ± 0.20 (1.75)	88	−1.08 ± 0.17 (1.60)	164	−1.25 ± 0.13 (1.69)
T_O from AMSRE	105	−2.13 ± 0.18 (1.81)	161	−1.64 ± 0.15 (1.86)	266	−1.76 ± 0.11 (1.86)
q_a (g/kg)						
AIRS	137	−0.73 ± 0.05 (0.71)	178	−0.66 ± 0.05 (0.68)	315	−0.69 ± 0.04 (0.70)
NCEP					585	0.12 ± 0.02 (0.46)

[a]Statistics are given separately for daytime (ascending satellite passes) and nighttime (descending) and for the total data set. Here "AIRS only" refers to the case in which both T_A and T_O were derived from AIRS. Abbreviations are as follows: AIRS, Atmospheric Infrared Sounder; AMSRE, Advanced Microwave Scanning Radiometer; NCEP, National Centers for Environmental Prediction.

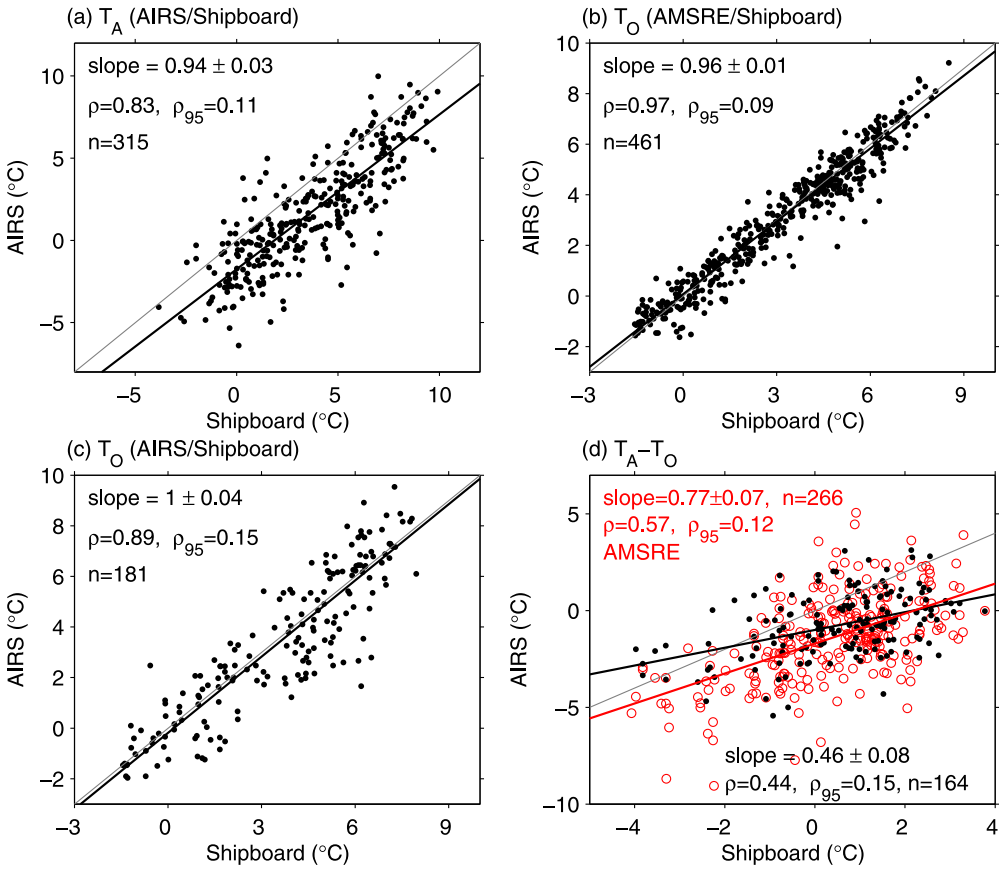

Figure 3. Scatterplots of (a) surface T_A from AIRS, (b) T_O from AMSRE, (c) T_O from AIRS, and (d) air-sea temperature difference from AIRS T_A minus AIRS T_O (dots) and AIRS T_A minus AMSRE T_O (circles) against the same quantities from shipboard measurements in the Drake Passage region. The thin gray line is the zero-bias line, and the thick black line is the linear regression of satellite retrievals to shipboard measurements. The slope of the regression lines, correlation coefficient (ρ) between satellite and shipboard data, and the corresponding value of the null correlation at 95% significance level (ρ_{95}) are listed. Units are °C.

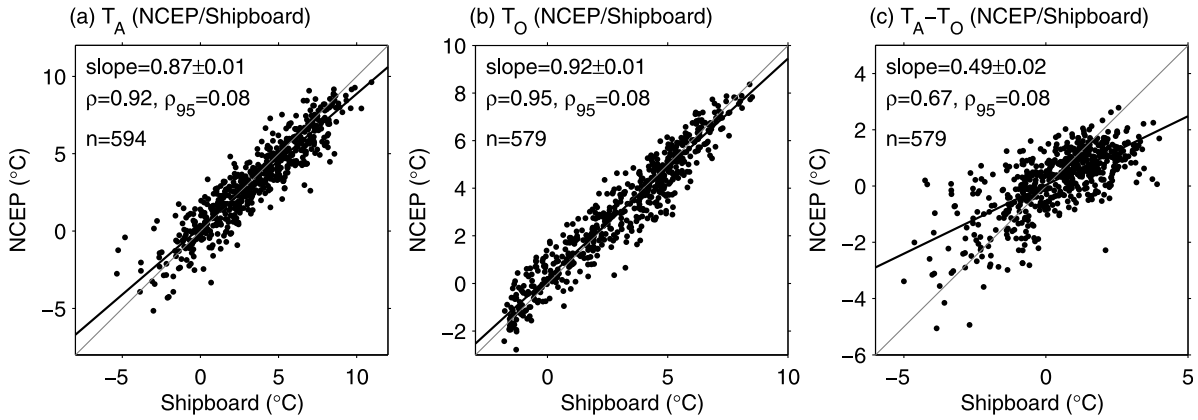

Figure 4. Scatterplots of NCEP (a) surface T_A, (b) T_O, and (c) $(T_A - T_O)$ against those from the shipboard measurements in the Drake Passage region. The gray lines are the zero-bias lines, and the thick solid lines are the linear regression of NCEP to shipboard. The slope of the regression lines, correlation coefficient (ρ) between NCEP and shipboard, and the corresponding 95% significance level of the correlation (ρ_{95}) are also indicated.

variability in NCEP air-sea temperature difference, and suggests that a sensible heat flux derived from the NCEP temperatures may not capture the flux variability as completely as a combination of AIRS and AMSRE.

3.2. Causes for the Biases in Temperature and Temperature Differences

[29] For the atmospheric boundary layer, if the ocean surface is colder than the overlying air, the atmosphere is stable. On the other hand, if the ocean surface is warmer than the overlying air, the near-surface air will warm and become less dense than the air above it, inducing convection. Thus, the air-sea temperature difference reflects the stability of the overlying atmosphere, which may also affect the AIRS retrievals [*Fetzer et al.* 2004]. Here the differences between the shipboard and the satellite data of near-surface air temperature ($\Delta T_{A,\mathrm{AIRS}} = T_{A,\mathrm{AIRS}} - T_{A,\mathrm{ship}}$ or $\Delta T_{A,\mathrm{NCEP}} = T_{A,\mathrm{NCEP}} - T_{A,\mathrm{ship}}$), sea surface temperature ($\Delta T_{O,\mathrm{AIRS}} = T_{O,\mathrm{AIRS}} - T_{O,\mathrm{ship}}$, $\Delta T_{O,\mathrm{AMSRE}} = T_{O,\mathrm{AMSRE}} - T_{O,\mathrm{ship}}$, or $\Delta T_{O,\mathrm{NCEP}} = T_{O,\mathrm{NCEP}} - T_{O,\mathrm{ship}}$), and air-sea temperature difference ($\Delta(T_A - T_O) = \Delta T_A - \Delta T_O$) are statistically examined against $(T_A - T_O)_{\mathrm{ship}}$. We also explore the dependence of these differences on T_A, T_O, q_a, cloud cover, and geographic location. Other factors, such as the vertical structure of atmospheric temperature and moisture, can also potentially influence the accuracy of the surface satellite retrievals. However, no accurate data source can be used to quantify their effects on the biases of near-surface satellite retrievals. Because of the relatively large mean bias in AIRS near-surface temperatures (Table 1), for both AIRS and AMSRE, the mean biases in T_A and T_O are removed before performing the statistical analysis.

[30] The statistical regression analyses (Figure 5a) suggest that $\Delta T_{A,\mathrm{AIRS}}$ has a significant dependence on $(T_A - T_O)_{\mathrm{ship}}$. Both the negative correlation between $\Delta T_{A,\mathrm{AIRS}}$ and $(T_A - T_O)_{\mathrm{ship}}$ and our regression analysis suggest that $\Delta T_{A,\mathrm{AIRS}}$ decreases with increasing $(T_A - T_O)_{\mathrm{ship}}$. In contrast, $\Delta T_{O,\mathrm{AIRS}}$ increases with increasing $(T_A - T_O)_{\mathrm{ship}}$, with twice the sensitivity of $\Delta T_{A,\mathrm{AIRS}}$ (Figure 5b). This is confirmed by the relatively large positive correlation of 0.31 between $\Delta T_{O,\mathrm{AIRS}}$ and $(T_A - T_O)_{\mathrm{ship}}$. In contrast, no significant correlation is found between $\Delta T_{O,\mathrm{AMSRE}}$ and $(T_A - T_O)_{\mathrm{ship}}$ (not shown). Both $\Delta(T_A - T_O)_{\mathrm{AIRS}}$ and $\Delta(T_A - T_O)_{\mathrm{AMSRE}}$ show significant correlations with $(T_A - T_O)_{\mathrm{ship}}$ (Figure 5c), which is to be expected considering the dependence of $\Delta T_{A,\mathrm{AIRS}}$ and $\Delta T_{O,\mathrm{AIRS}}$ on $(T_A - T_O)_{\mathrm{ship}}$ (Figures 5a and 5b). Our regression analysis suggests that the dependence of $\Delta(T_A - T_O)_{\mathrm{AIRS}}$ on $(T_A - T_O)_{\mathrm{ship}}$ is more than twice as strong as the dependence of $\Delta(T_A - T_O)_{\mathrm{AMSRE}}$ on $(T_A - T_O)_{\mathrm{ship}}$, which is also suggested by the strong dependence of $\Delta T_{O,\mathrm{AIRS}}$ on $(T_A - T_O)_{\mathrm{ship}}$. Further analysis suggests that the temperature biases depend significantly on $T_{A,\mathrm{ship}}$ but not on $T_{O,\mathrm{ship}}$. The dependence of temperature biases on $T_{A,\mathrm{ship}}$ is similar to their dependence on $(T_A - T_O)_{\mathrm{ship}}$, although it is relatively weak.

[31] Infrared measurements are strongly influenced by water vapor and cloud cover. *Susskind et al.* [2006] found that AIRS retrieval accuracy degrades slightly with increasing cloud cover. Our statistical analyses suggest that ΔT_A, ΔT_O, and $\Delta(T_A - T_O)$ are not affected by cloud cover, but all three are affected similarly by AIRS-derived water vapor, column total water vapor from AMSRE, and shipboard RH. Thus, here we describe only the dependence of temperature differences on shipboard RH measurements. Figure 5d shows that $\Delta T_{A,\mathrm{AIRS}}$ is positively correlated with RH (dashed line). For satellite-derived ocean temperatures the relationship is less pronounced: $\Delta T_{O,\mathrm{AIRS}}$ does not depend on RH (Figure 5e), and $\Delta T_{O,\mathrm{AIRS}}$ shows a weak but significant negative correlation with RH (not shown), consistent with the negative correlation between $\Delta T_{O,\mathrm{AMSRE}}$ and column water vapor reported by *Dong et al.* [2006a]. Because satellite retrievals of T_A and T_O depend on RH, both $\Delta(T_A - T_O)_{\mathrm{AIRS}}$ and $\Delta(T_A - T_O)_{\mathrm{AMSRE}}$ are positively correlated with RH (Figure 5f) at a statistically significant level.

[32] Our analysis also suggests that $\Delta T_{O,\mathrm{AIRS}}$ depends on q_a (Figure 5h). As q_a increases, $\Delta T_{O,\mathrm{AIRS}}$ tends to increase. $\Delta T_{O,\mathrm{AMSRE}}$ also experiences significant dependence on q_a (not shown), but in an opposite sense to $\Delta T_{O,\mathrm{AIRS}}$: an

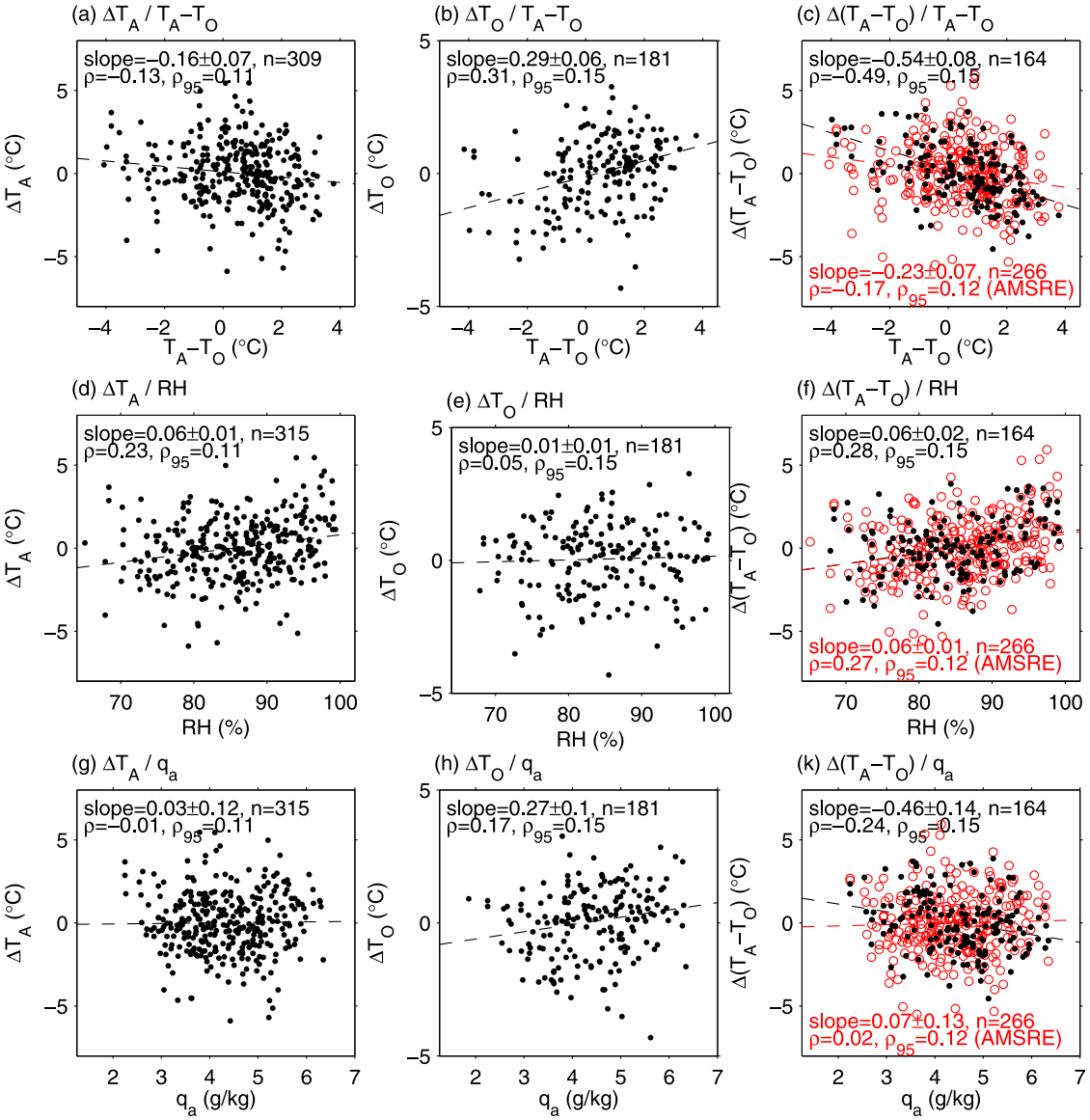

Figure 5. Scatterplots of (a) $\Delta T_{A,AIRS}$, (b) $\Delta T_{O,\mathrm{AIRS}}$, and (c) $\Delta(T_A - T_O)_{\mathrm{AIRS}}$ (dots) and $\Delta(T_A - T_O)_{\mathrm{AMSRE}}$ (circles) against the air-sea temperature difference determined from shipboard measurements. The dashed lines are the linear regression of AIRS/AMSRE to shipboard $(T_A - T_O)_{\mathrm{ship}}$. (d–f) Same as Figures 5a–5c except against shipboard relative humidity; (g–k) same as Figures 5a–5c except against specific humidity. The slope of the regression lines, correlation coefficient (ρ), and the corresponding 95% significance level of the correlation (ρ_{95}) are also indicated.

increase in q_a would cause a decrease in $\Delta T_{O,\mathrm{AMSRE}}$. Although T_A is closely related to q_a, no significant dependence of $\Delta T_{A,\mathrm{AIRS}}$ on q_a was found (Figure 5g). $\Delta(T_A - T_O)_{\mathrm{AIRS}}$ decreases with increasing q_a because of the dependence of $\Delta T_{O,\mathrm{AIRS}}$ on q_a (Figure 5k). However, $\Delta(T_A - T_O)_{\mathrm{AMSRE}}$ does not experience a statistically significant relationship with q_a.

[33] As in the rest of the Southern Ocean, the Antarctic Circumpolar Current that passes through Drake Passage is characterized by strong meridional gradients in temperature that result in sharp fronts. We therefore considered the possibility that ΔT_A, ΔT_O, and $\Delta(T_A - T_O)$ have a cross-passage bias in response to the frontal positions. No simple linear dependence of the temperature biases on latitude and longitude was found. We will further examine the cross-passage dependence of ΔT_A, ΔT_O, and $\Delta(T - T_O)$ in section 5.

4. Evaluation of AIRS Surface Specific Humidity

4.1. Comparison of Near-Surface Specific Humidity

[34] On average, AIRS surface q_a has a negative bias of −0.69 g/kg compared with shipboard measurements (Table 1). The q_a difference between AIRS and shipboard measurements shows a marginal difference between daytime (−0.73 g/kg) and nighttime (−0.66 g/kg) (Table 1). The difference between the AIRS q_a and shipboard q_a for each collocated pair varies between −4.2 and 2.3 g/kg. Regressing AIRS q_a to shipboard q_a measurements gives a slope of 0.89

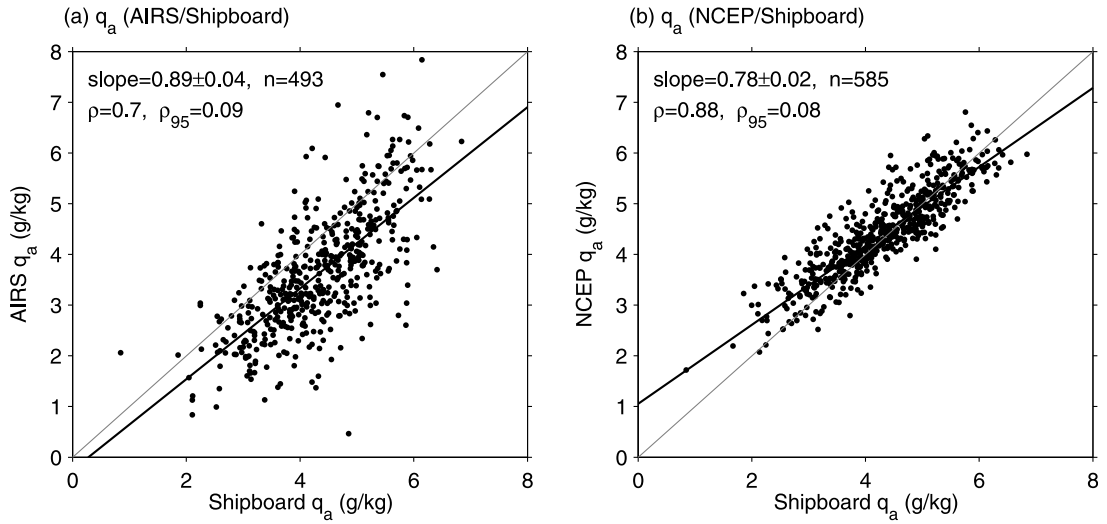

Figure 6. Scatterplots of specific humidity from (a) AIRS and (b) NCEP against specific humidity derived from shipboard measurements in the region across the Drake Passage. The linear regression is shown as the thick black line, and the gray line is the zero bias. The slope of the regression lines, correlation coefficient (ρ), and the corresponding 95% significance level of the correlation (ρ_{95}) are also indicated.

(Figure 6a), suggesting that the AIRS q_a captures the observed q_a variability.

[35] To examine the relative performance of AIRS q_a measurements, we also compared the NCEP q_a with shipboard q_a measurements. The mean difference between NCEP and the shipboard q_a measurements is small, with NCEP q_a higher than shipboard measurements by 0.12 g/kg on average (Table 1). The difference between NCEP q_a and shipboard q_a for each collocated pair varies between −1.1 and +1.5 g/kg (Figure 6b). Like the AIRS measurements (Figure 6a), NCEP q_a measurements are also significantly correlated with shipboard q_a measurements (ρ = 0.88). The scatterplot of the NCEP q_a versus shipboard q_a (Figure 6b) shows that the scatter of the data is relatively small compared to that of the AIRS q_a versus shipboard q_a (Figure 6a). This is consistent with the smaller RMS error of NCEP q_a compared with the RMS error of AIRS q_a (Table 1). Thus, whether the AIRS q_a can improve the latent heat flux estimate still remains in question.

4.2. Causes for the Biases in AIRS Specific Humidity

[36] We examined the dependence of the difference in near-surface specific humidity ($\Delta q_a = q_{a,\mathrm{AIRS}} - q_{a,\mathrm{ship}}$) between AIRS and shipboard measurements on T_A, T_O, $(T_A - T_O)$, q_a, cloud cover, RH, and geographic location. Similar to the near-surface temperature, the mean bias in AIRS q_a is removed before performing the statistical analyses. Results from the statistical analyses suggest that Δq_a decreases with increasing $(T_A - T_O)_{\mathrm{ship}}$, and the dependence of Δq_a on $(T_A - T_O)_{\mathrm{ship}}$ is stronger for cases when the air-sea temperature difference is positive (Figure 7a).

[37] Statistical analyses of Δq_a against AIRS cloud fraction measurements suggest that Δq_a has a significant

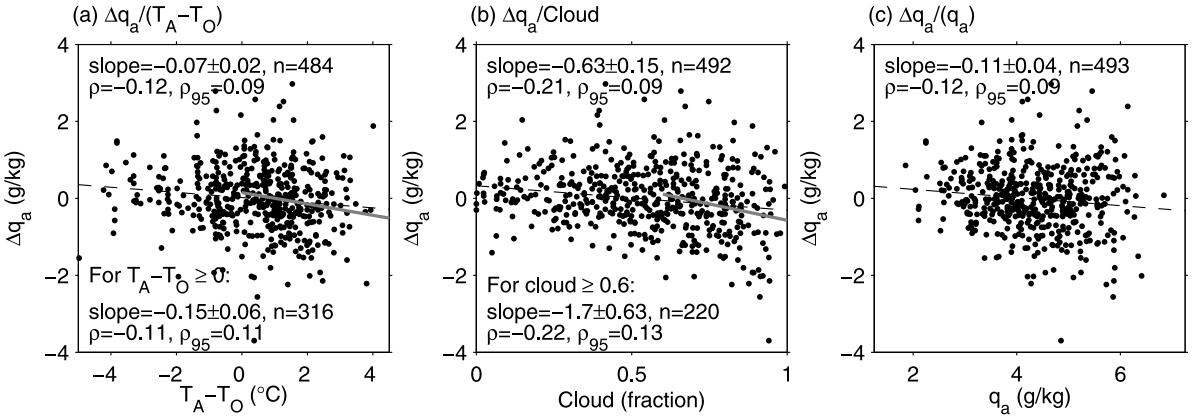

Figure 7. Scatterplots of Δq_a (AIRS minus shipboard) against (a) shipboard measurements of $T_A - T_O$, (b) AIRS cloud fraction, and (c) shipboard q_a. The linear regression is shown as a dashed line. The gray line corresponds to the linear regression for cases where $T_A - T_O > 0$ in Figure 7a and for cases where cloud fraction exceeds 0.6 in Figure 7b. Units are °C for temperature and g/kg for q_a.

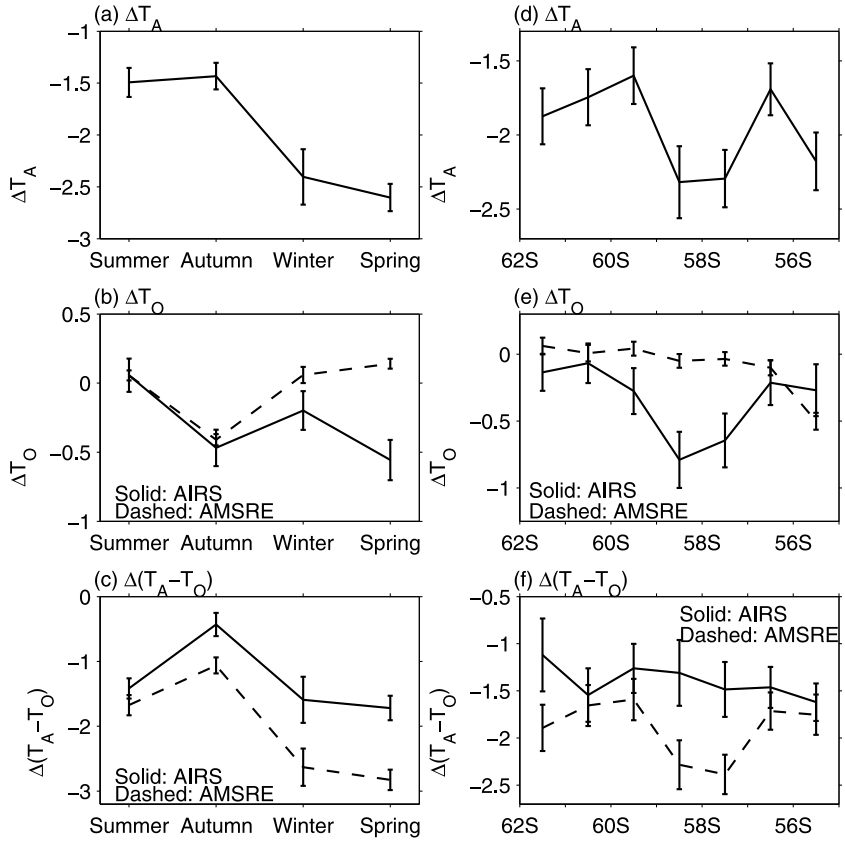

Figure 8. Three month averages of (a) $\Delta T_{A,AIRS}$, (b) $\Delta T_{O,AIRS}$ (solid line), and $\Delta T_{O,\mathrm{AMSRE}}$ (dashed line), and (c) $\Delta(T_A - T_O)_{AIRS}$ (solid line) and $\Delta(T_A - T_O)_{\mathrm{AMSRE}}$ (dashed line). (d–f) Same as in Figures 8a–8c except for averages at each latitude in Drake Passage. The corresponding standard errors are indicated by the vertical lines.

dependence on cloud (Figure 7b), with a significant negative correlation of −0.21, exceeding the 95% significance level of 0.09. The dependence of Δq_a on cloud is relatively strong for cases with a cloud fraction exceeding 0.6, whereas for cases with cloud fraction lower than 0.6 the dependence is less apparent. Linear regression of Δq_a to the cloud fraction suggests that an increase in cloud fraction causes a more negative bias in the AIRS q_a.

[38] We also found a significant dependence of Δq_a on q_a itself (Figure 7c). As q_a increases, Δq_a decreases. Because of the overall negative bias in AIRS q_a, this suggests that AIRS q_a has more negative bias for cases with relatively higher q_a. In terms of percentage, we found that the time mean error of q_a is about 21% of q_a, consistent with the results of *Tobin et al.* [2006].

5. Seasonal and Cross-Passage Variations in AIRS Biases

5.1. Surface Temperatures

[39] The biases in the daytime and nighttime temperature retrievals from AIRS and AMSRE only differ marginally from each other, as suggested by their comparison with shipboard measurements (Table 1). However, ΔT_A, ΔT_O, and $\Delta(T_A - T_O)$ show strong seasonal differences (Figure 8a–8c). The cold bias in AIRS T_A is largest in austral spring and smallest in autumn. AIRS T_O has a cold bias except in austral summer, when $\Delta T_{O,\mathrm{AIRS}}$ is positive but very small. In contrast, $\Delta T_{O,\mathrm{AMSRE}}$ is relatively small and is positive during summer, winter, and spring but negative in autumn. The seasonal biases in temperature cannot be explained simply by their dependence on $T_A - T_O$, RH, and q_a. Shipboard RH shows little seasonal variations; thus it could not contribute to the seasonal changes in the temperature biases. Specific humidity derived from shipboard measurements is relatively high during summer but not significantly different in the other three seasons, suggesting that the contribution of q_a to seasonal biases in temperature is also limited. Although the large, negative $T_A - T_O$ during autumn can explain the less negative bias in $\Delta T_{A,\mathrm{AIRS}}$, the stronger, positive $T_A - T_O$ during summer implies a more negative bias in $\Delta T_{A,\mathrm{AIRS}}$ compared to other seasons, the opposite of that shown in Figure 8a.

[40] Figures 9d–9f show the averages of ΔT_A, ΔT_O, and $\Delta(T_A - T_O)$ at each latitude grid regardless of the longitudinal location. Both T_A (Figure 8d) and T_O (Figure 8e, solid) from AIRS are cooler than the shipboard measurements at all latitudes from 55.5°S to 61.5°S. The maximum differences occur in the region between 57°S and 59°S, coinciding with the general location of the Polar Front in Drake Passage [*Sprintall*, 2003]. As shown in section 3, both temperature and humidity affect AIRS temperature retrievals; hence the large difference between AIRS and shipboard temperature measurements in the frontal region may be

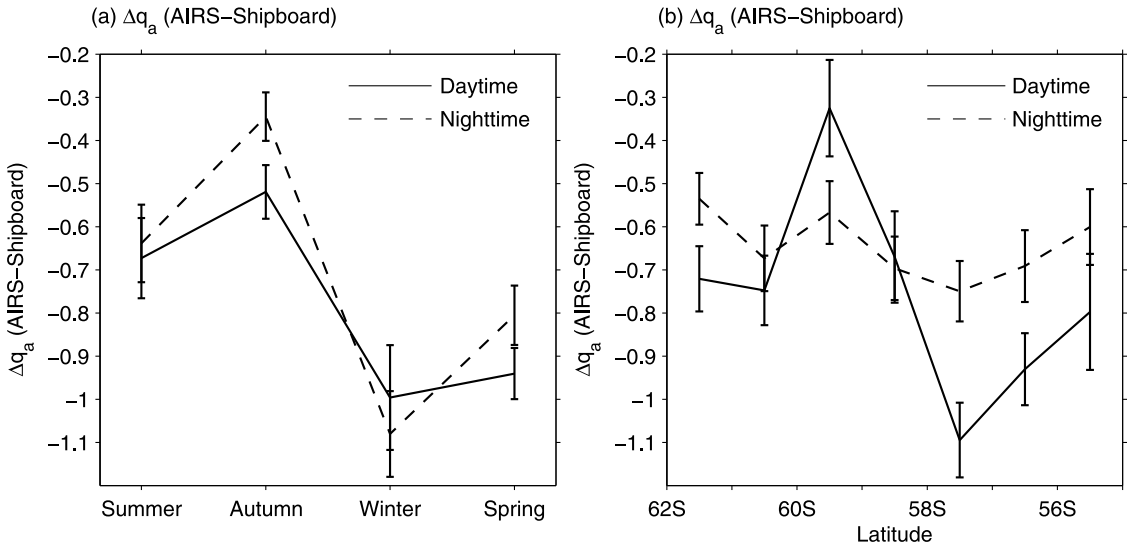

Figure 9. (a) Three month averaged Δq_a (AIRS minus shipboard) and (b) Δq_a averaged in 1° latitude bins. Solid and dashed lines are for daytime and nighttime, respectively. The corresponding standard errors are indicated by the vertical lines.

related to the strong horizontal gradient in both the temperature and humidity fields. Because of the similarity of the latitudinal distribution of $\Delta T_{A,\mathrm{AIRS}}$ and $\Delta T_{O,\mathrm{AIRS}}$, $\Delta(T_A - T_O)_{\mathrm{AIRS}}$ does not have significant cross-passage variation (Figure 8f, solid line), although the overall trend is for smaller values to the north. In general, $\Delta T_{O,\mathrm{AMSRE}}$ (Figure 8e, dashed line) is much smaller than $\Delta T_{O,\mathrm{AIRS}}$, with positive values south of 59°S and negative values to the north. The cross-passage distribution of $\Delta(T_A - T_O)_{\mathrm{AMSRE}}$ (Figure 8f, dashed line) is similar to that of ΔT_A due to the dominance of the cold bias in AIRS T_A.

5.2. Near-Surface Specific Humidity

[41] Like near-surface temperature differences, Δq_a also shows a seasonal variation (Figure 9a). Both daytime and nighttime Δq_a are negative for all seasons, with more negative biases during austral winter and spring. This seasonal bias cannot be explained by the dependence of Δq_a on the air-sea temperature difference and cloud fraction: the more positive air-sea temperature difference and the relatively high cloud fraction (not shown) during summer imply a more negative bias compared to winter and spring, the opposite of that shown in Figure 9a. The less negative bias during summer might be related to the fact that there are more summer shipboard samples available south of 59°S, where the negative bias is relatively small (Figure 9b). The daytime Δq_a is more negative compared to the nighttime Δq_a, except during winter. The larger daytime bias is potentially related to the more positive air-sea temperature difference and slightly higher cloud fraction during the daytime (not shown). The average Δq_a at each latitude grid point (Figure 9b) suggests that the bias in the AIRS q_a becomes more negative from south to the north across the Drake Passage during both daytime and nighttime, which may be related to the increase in the cloud fraction to the north. The daytime Δq_a also shows a large gradient between 57°S and 59°S that coincides with the location of the oceanic frontal region where the temperature gradient is large (Figure 2). The reason for this cross-passage variability in the daytime q_a bias is unclear and calls for further examination in future studies.

6. Uncertainties in Turbulent Heat Fluxes From AIRS/Advanced Microwave Scanning Radiometer Surface Retrievals

[42] To examine whether AIRS near-surface T_A, T_O, and q_a retrievals are accurate enough to use in turbulent heat flux estimations, we compute the sensible (equation (1)) and latent (equation (2)) heat fluxes from the COARE3.0 algorithm using the collocated T_A, T_O, and q_a from AIRS, AMSRE, NCEP, and shipboard measurements. Here we focus on the uncertainties in turbulent heat fluxes stemming from using satellite T_A, T_O, and q_a retrievals, and therefore all other variables required in equations (1) and (2) are the same for each estimate. The collocation process for these other NCEP variables (e.g., q_s, W, and ρ_a) is the same as that outlined in section 2. We use either shipboard or NCEP winds in the computation, as discussed below. The COARE algorithm was initially developed for the tropics, without high-latitude data or high wind conditions [*Fairall et al.*, 1996]. Although high-latitude data were used in developing and validating the updated versions 2.6 and 3.0, no data were available from the Southern Ocean [*Fairall et al.*, 2003]. Thus, the algorithm's performance in the Southern Ocean still needs to be assessed. However, since the main purpose of this study is to evaluate the AIRS surface retrievals, for simplicity we use the COARE3.0 algorithm directly, as it is the most widely used algorithm currently available.

[43] Four different sensible and latent heat fluxes are estimated, including those based on T_A, T_O, and q_a from shipboard measurements ($\mathrm{SH_{ship}}$, $\mathrm{LH_{ship}}$), from NCEP ($\mathrm{SH_{NCEP}}$, $\mathrm{LH_{NCEP}}$), and from AIRS ($\mathrm{SH_{AIRS}}$, $\mathrm{LH_{AIRS}}$). The fourth is based on AMSRE T_O and AIRS T_A and q_a ($\mathrm{SH_{AMSRE}}$, $\mathrm{LH_{AMSRE}}$). Here $\mathrm{SH_{ship}}$ and $\mathrm{LH_{ship}}$ are consid-

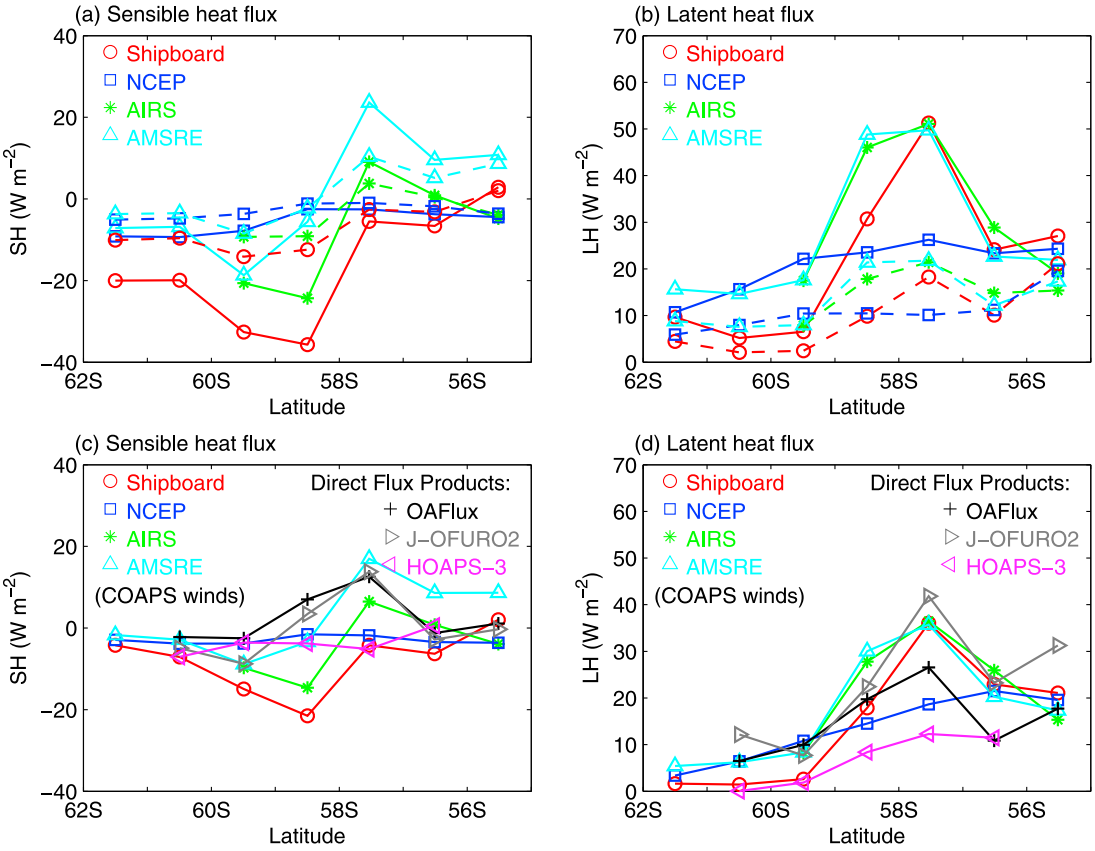

Figure 10. (a) Sensible and(b) latent heat fluxes estimated from the Coupled Ocean-Atmospheric Response Experiment bulk flux algorithm version 3.0 using the collocated near-surface parameters for a Drake Passage crossing during October 2005, the same crossing as in Figure 2. The fluxes are estimated from shipboard measurements (red), NCEP parameters (blue), the AIRS T_A, T_O, and q_a (green), and AIRS T_A, q_a, and AMSRE T_O (cyan). Dashed lines are the fluxes estimated using NCEP winds, and solid lines correspond to the fluxes estimated using shipboard winds. (c and d) Same as Figures 10a and 10b but also include fluxes directly from Objectively Analyzed air-sea Fluxes (OAFlux) (black), Japanese Ocean Flux data sets with Use of Remote sensing Observations version (2J-OFURO2) (gray), and Hamburg ocean atmosphere parameters and fluxes from satellite data (HOAPS-3) (magenta). In Figures 10c and 10d, QuikSCAT wind speeds from Center for Ocean-Atmospheric Prediction Studies were used in the turbulent heat flux estimates that used the shipboard, AIRS, AMSRE, and NCEP data. Units are W/m^2.

ered as "truth" and are used to evaluate the uncertainties in the other three estimations. The fluxes are defined as positive out of the ocean. The mean biases in AIRS/AMSRE and NCEP T_A, T_O, and q_a (Table 1) are removed prior to the flux estimation. Figure 10 shows an example of the turbulent heat fluxes for the October 2005 LMG Drake Passage crossing shown in Figure 2. As we found for the individual parameters (Figure 2), both SH_{NCEP} and LH_{NCEP} are consistently too smooth to capture the variability in SH_{ship} and LH_{ship}. In contrast, both SH_{AMSRE} and LH_{AMSRE} show good representation of the variability in SH_{ship} and LH_{ship} across the Drake Passage, except at grid points at the southern and northern boundaries, where land/ice effects may bias satellite retrievals. Although mean biases of all the collocated pairs have been removed, there is a residual bias of −1.10°C in AIRS T_A and 0.35°C in AMSRE T_O for this particular crossing, which explains the positive biases in both SH_{AMSRE} and LH_{AMSRE}. In this case, the available SH_{AIRS} agrees better with SH_{ship} than SH_{NCEP} in showing the sharp cross-passage gradients of the fluxes and the negative values south of 58°S. The agreement of LH_{AIRS} with LH_{ship} is also better than that between LH_{NCEP} and LH_{ship} (Figure 10b). The fluxes increase by a factor of 2–3, and the distinctions are more dramatic when we use more realistic shipboard winds (solid lines) rather than NCEP winds (dashed lines), underscoring the sensitivity of turbulent heat fluxes to wind speed.

[44] The overall comparison of the turbulent flux estimations from AIRS, AMSRE, and NCEP against those from all the shipboard measurements is given in Figure 11. All comparisons use the shipboard winds. SH_{AIRS} experiences the smallest RMS error compared with SH_{ship} (Figure 11a). However, SH_{AMSRE} demonstrates the best performance in terms of capturing the full range of values of the SH_{ship}, suggested by the large slope (0.78) of the regression line (Figure 11b). SH_{AIRS} (Figure 11a) performs slightly better than SH_{NCEP} (Figure 11c) in capturing the full range of values of the SH_{ship}. The comparison of LH shows results similar to those from the SH comparison: LH_{AIRS} has smaller RMS errors than LH_{NCEP} (Figure 11d,f), and

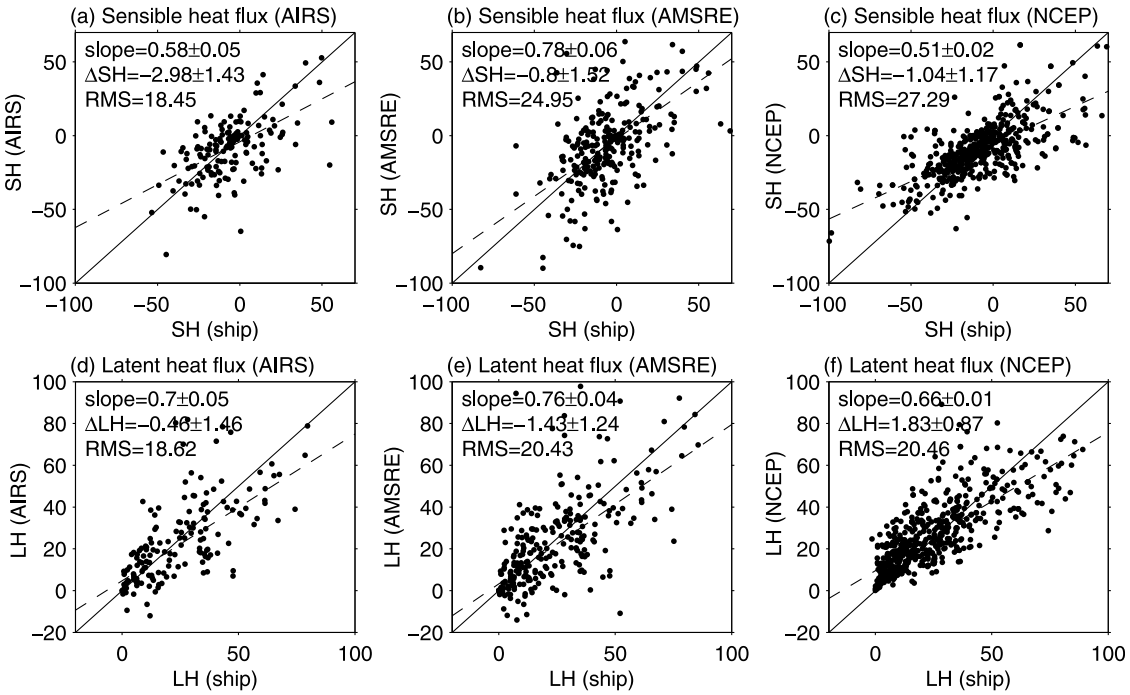

Figure 11. Scatterplots of sensible heat fluxes determined from COARE3.0 using (a) AIRS T_A, T_O, and q_a, (b) AIRS T_A and q_a and AMSRE T_O, and (c) NCEP near-surface parameters against the sensible heat fluxes estimated using shipboard measurements. (d–f) Same as Figures 11a–11c but for latent heat fluxes. Shipboard winds are used in the flux estimates. The solid line is the zero-bias line, and the dashed line is the linear regression. The slope of the regression lines, mean difference in sensible (ΔSH) and latent (ΔLH) heat fluxes between those from satellite/NCEP parameters and those from shipboard measurements, and the corresponding root-mean-square error (RMS) are listed. Units are W/m^2.

LH_{AMSRE} demonstrates the best performance in terms of capturing the full range of values of the LH_{ship} (Figure 11e). However, the RMS error of all three latent heat flux estimates (LH_{AIRS}, LH_{AMSRE}, and LH_{NCEP}) differs only marginally. Considering both the RMS errors and the ability to capture the full range of LH_{ship} and SH_{ship} values, we conclude that the turbulent heat flux estimates from the AIRS/AMSRE combination perform better than those from AIRS alone and NCEP.

[45] Finally, to examine the potential of AIRS surface retrievals in improving flux estimates, we also compare existing satellite-derived flux products, OAFlux, J-OFURO2, and HOAPS-3, with the sensible (Figure 10c) and latent (Figure 10d) heat fluxes estimated from shipboard measurements. Because of the strong sensitivity of the turbulent heat fluxes to the choice of wind speed (e.g., Figures 10a and 10b) and the fact that scatterometers are one of the main wind data sources in the existing flux products, we used the QuickSCAT wind speed from COAPS in calculating LH and SH from the shipboard, AIRS, AMSRE, and NCEP variables to give a fair comparison. For the case shown in Figure 10, the sensible heat fluxes from both OAFlux and J-OFURO2 compare well with SH_{ship}, although SH_{AMSRE} performs slightly better in terms of the cross-passage variations in SH_{ship}. HOAPS-3 fluxes perform similarly to SH_{NCEP} and LH_{NCEP}, which are consistently too smooth to capture the variability in SH_{ship} and LH_{ship}. The latent heat flux from J-OFURO2 performs similarly to LH_{AIRS} and LH_{AMSRE} and best captures the cross-passage variations in LH_{ship}; however, it deviates from LH_{ship} near the boundaries and experiences the largest RMS error. LH from OAFlux captures about half of the cross-passage variations in LH_{ship} for this cruise.

[46] Table 2 summarizes the RMS errors and regression slopes of the turbulent flux estimates from AIRS, AMSRE, and NCEP parameters and those from the existing flux products in comparison with the flux estimates from the shipboard parameters. The sensible heat fluxes from the OAFlux and J-OFURO2 have the smallest the RMS errors. However, SH_{AMSRE} performs best at capturing the full range of values of SH_{ship}, with a regression slope closest to 1 (Table 2). In the latent heat flux comparison, LH_{AMSRE} and $LH_{J\text{-}OFURO2}$ perform better in capturing the range of the LH_{ship} variations. However, $LH_{J\text{-}OFURO2}$ has the largest RMS errors. LH_{NCEP} has the smallest RMS error, but LH_{NCEP} does the poorest in capturing the full range of variations. Given the different performance in terms of RMS error and different skill in capturing the full range of shipboard estimates (Table 2), it is difficult to determine which flux products best represent the "truth." The AIRS/AMSRE combination best represents the full range of shipboard values for both LH and SH, whereas the OAFlux and J-OFURO2 products have the smallest RMS error for SH, and OAFlux and NCEP have the smallest RMS error for LH. Our results therefore suggest that for studies focusing on the mean climate state in the Southern Ocean, OAFlux and NCEP may provide better turbulent heat flux values. However, for those studies focused on climate variability,

Table 2. Root-Mean-Square Error and Regression Slope of the Turbulent Heat Flux From Various Satellite and Existing Flux Products Against Those Fluxes Calculated From Shipboard Variables of Near-Surface Air Temperature, Ocean Temperature, and Specific Humidity[a]

	Sensible Heat Flux (W/m^2)		Latent Heat Flux (W/m^2)	
	RMS Error	Slope	RMS Error	Slope
AIRS	19.31	0.53 ± 0.06	19.01	0.79 ± 0.07
AIRS/AMSRE	21.88	0.73 ± 0.06	18.96	0.84 ± 0.05
NCEP	16.69	0.47 ± 0.02	10.68	0.59 ± 0.02
OAFlux	15.50	0.60 ± 0.03	17.01	0.78 ± 0.04
J-OFURO2	15.62	0.58 ± 0.03	26.70	0.88 ± 0.07
HOAPS-3	25.23	0.22 ± 0.03	23.17	0.72 ± 0.07

[a]QuikSCAT wind speeds from Center for Ocean-Atmospheric Prediction Studies were used in the turbulent heat flux estimates that used the shipboard, AIRS, AMSRE, and NCEP data. Abbreviations are as follows: HOAPS-3, Hamburg ocean atmosphere parameters and fluxes from satellite data; J-OFURO2, Japanese Ocean Flux data sets with Use of Remote sensing Observations version 2; OAFlux, Objectively Analyzed air-sea Fluxes; RMS, root-mean-square.

AIRS and AMSRE measurements have the potential to provide the best turbulent flux estimations.

7. Discussion and Conclusions

[47] Satellite measurements have played a major role in estimating air-sea heat fluxes because of their spatial and temporal coverage. Remotely sensed sea surface temperature and wind speed have become standard in the estimation of sensible and latent heat flux components. More recently, near-surface air temperature and specific humidity have been made available from AIRS, an infrared sounder on board the Aqua satellite. In this study, we evaluate whether the near-surface air temperature, sea surface temperature, their difference, and specific humidity from AIRS are suitable for estimating latent and sensible heat fluxes from bulk formula. Our evaluation is undertaken in the Southern Ocean, where existing air-sea heat flux products have large uncertainties [*Dong et al.*, 2007]. The evaluation is done by comparing the near-surface AIRS observations with in situ shipboard meteorological observations in the Drake Passage. Since sensible heat flux estimates depend on air-sea temperature differences, we also consider T_O from AMSRE with the shipboard observations.

[48] Overall, our comparison indicates that, in cases with minimal cloud/water vapor contamination when the AIRS near-surface parameters are mostly available for the entire region, AIRS and AMSRE together can provide a better representation of the spatial variation evident in the shipboard measurements in the Drake Passage compared to the much smoother NCEP data. Although the AIRS surface temperature retrievals have relatively large cold biases, our comparison to shipboard measurements indicates that AIRS temperatures follow the variations in shipboard measurements with regression slopes close to 1.0. In particular, the satellite-derived air-sea temperature differences (with AIRS T_A minus AMSRE T_O) versus those from shipboard measurements follow the zero-bias line more closely than do NCEP air-sea temperature differences. This suggests that satellite measurements have the potential to provide better parameters for the sensible heat flux bulk formula, largely because they capture the full range of values in Drake Passage. However, it is still in question whether the AIRS specific humidity values can improve the latent heat flux estimates in the Southern Ocean, in view of the relatively large deviations of AIRS q_a from the shipboard measurements. Nevertheless, turbulent heat flux estimates using the COARE3.0 algorithm indicate that the AIRS/AMSRE combination does a better job than the existing reanalysis or satellite-derived heat fluxes at capturing the full range of turbulent heat flux values from the Drake Passage shipboard observations.

[49] The present study is focused on the AIRS L3 gridded products. AIRS level 2 (L2, swath data) products have a higher spatial resolution in both vertical and horizontal directions, which may better represent some of the small-scale variability. It is also straightforward to combine the simultaneous measurements of AIRS L2 T_A and q_a with AMSRE T_O and winds for turbulent flux estimates, which may give the best possible agreement with the full range of shipboard observations in Drake Passage (Table 2). *Jackson et al.* [2006] suggested that combining two or three microwave sensors could improve near-surface air temperature and specific humidity retrievals. Our analysis for the Drake Passage gives the RMS error of 1.83°C in T_A and 0.70 g/kg for q_a. These RMS errors are lower than the RMS error of 1.96°C for T_A and 0.94 g/kg for q_a reported by *Jackson et al.* [2006] when merging two or three microwave sensors. However, their data were all from the tropical and subtropical regions north of 10°S, with a large range of T_A from 5°C to 29°C and q_a from 3 to 19 g/kg. In contrast, our Southern Ocean study region of colder T_A and lower q_a covered a smaller range from −3°C to 11°C for T_A and from 0.8 to 7 g/kg for q_a. Supporting the findings of *Jackson et al.* [2006], our ongoing analysis also suggests that AIRS performs relatively better in the tropics compared to the Southern Ocean (not shown), suggesting that a multisensor method merging AIRS and microwave SST may yield even better results using near-surface temperature and humidity data to estimate turbulent heat flux.

[50] **Acknowledgments.** We thank the two anonymous reviewers for their insightful comments. The AIRS version 5 level 3 daily products are distributed by the Goddard Earth Sciences Distributed Active Archive Center at http://disc.sci.gsfc.nasa.gov/AIRS/. NCEP/NCAR Reanalysis data are provided by the NOAA/OAR/ESRL PSD from their Web site at http://www.cdc.noaa.gov/. AMSRE data are produced by Remote Sensing Systems and sponsored by the NASA Earth Science REASoN DISCOVER Project and the AMSRE Science Team and are available from http://www.ssmi.com/. The HOAPS data are provided by the World Data Center for Climate, Hamburg, Germany. The OAFlux is from http://oaflux.whoi.edu. J-OFURO2 data are obtained from the J-OFURO2 Web site http://dtsv.scc.u-tokai.ac.jp/J-OFURO2/. This research is supported by NOAA/AOML and by grants from the National Science Foundation (Office of Polar Programs Award 0337998 and OCE Award 0850350).

References

Andersson, A., S. Bakan, and C. Klepp (2007), The HOAPS climatology, *Flux News*, *4*, 10–12.

Aumann, H. H., et al. (2003), AIRS/AMSU/HSB on the Aqua mission: Design, science objectives, data products, and processing systems, *IEEE Trans. Geosci. Remote Sens.*, *41*(2), 253–264, doi:10.1109/TGRS.2002.808356.

Aumann, H. H., S. Broberg, D. Elliott, S. Gaiser, and D. Gregorich (2006), Three years of Atmospheric Infrared Sounder radiometric calibration validation using sea surface temperatures, *J. Geophys. Res.*, *111*, D16S90, doi:10.1029/2005JD006822.

Barsguli, J., and D. S. Battisti (1998), The basic effects of atmosphere-ocean thermal coupling on midlatitude variability, *J. Atmos. Sci.*, *55*, 477–493, doi:10.1175/1520-0469(1998)055<0477:TBEOAO>2.0.CO;2.

Barton, I. J., P. J. Minnett, K. A. Maillet, C. J. Donlon, S. J. Hook, A. T. Jessup, and T. J. Nightingale (2004), The Miami2001 infrared radiometer calibration and inter-comparison: 2. Ship-board results, *J. Atmos. Oceanic Technol.*, *21*, 268–283, doi:10.1175/1520-0426(2004)021<0268:TMIRCA>2.0.CO;2.

Bentamy, A., K. B. Katsaros, M. Alberto, W. M. Drennan, E. B. Forde, and H. Roquet (2003), Satellite estimates of wind speed and latent heat flux over the global oceans, *J. Clim.*, *16*, 637–656, doi:10.1175/1520-0442(2003)016<0637:SEOWSA>2.0.CO;2.

Ciasto, L. M., and D. W. J. Thompson (2008), Observations of large-scale ocean-atmosphere interaction in the Southern Hemisphere, *J. Clim.*, *21*, 1244–1259, doi:10.1175/2007JCLI1809.1.

Curry, J. A., et al. (2004), SEAFLUX, *Bull. Am. Meteorol. Soc.*, *85*, 409–424, doi:10.1175/BAMS-85-3-409.

Divakarla, M., C. Barnet, M. D. Goldberg, L. McMillin, E. S. Maddy, W. W. Wolf, L. Zhou, and X. Liu (2006), Validation of Atmospheric Infrared Sounder temperature and water vapor retrievals with matched radiosonde measurements and forecasts, *J. Geophys. Res.*, *111*, D09S15, doi:10.1029/2005JD006116.

Dong, S., S. T. Gille, J. Sprintall, and C. Gentemann (2006a), Validation of Advanced Microwave Scanning Radiometer for the Earth Observing System (AMSR-E) sea surface temperature in the Southern Ocean, *J. Geophys. Res.*, *111*, C04002, doi:10.1029/2005JC002934.

Dong, S., J. Sprintall, and S. T. Gille (2006b), Location of the Antarctic polar front from AMSR-E satellite sea surface temperature measurements, *J. Phys. Oceanogr.*, *36*, 2075–2089, doi:10.1175/JPO2973.1.

Dong, S., S. T. Gille, and J. Sprintall (2007), An assessment of the Southern Ocean mixed-layer heat budget, *J. Clim.*, *20*, 4425–4442, doi:10.1175/JCLI4259.1.

Fairall, C. W., E. F. Bradley, D. P. Rogers, J. B. Edson, and G. S. Young (1996), Bulk parameterization of air-sea fluxes for TOGA-COARE, *J. Geophys. Res.*, *101*, 3747–3764, doi:10.1029/95JC03205.

Fairall, C. W., E. F. Bradley, J. E. Hare, A. A. Grachev, and J. B. Edson (2003), Bulk parameterization of air-sea fluxes: Updates and verification for the COARE algorithm, *J. Clim.*, *16*, 571–591, doi:10.1175/1520-0442(2003)016<0571:BPOASF>2.0.CO;2.

Fetzer, E. J. (2006), Preface to special section: Validation of Atmospheric Infrared Sounder Observations, *J. Geophys. Res.*, *111*, D09S01, doi:10.1029/2005JD007020.

Fetzer, E. J., J. Teixeira, E. T. Olsen, and E. F. Fishbein (2004), Satellite remote sounding of atmospheric boundary layer temperature inversions over the subtropical eastern Pacific, *Geophys. Res. Lett.*, *31*, L17102, doi:10.1029/2004GL020174.

Gentemann, C. L., F. J. Wentz, C. A. Mears, and D. K. Smith (2004), In situ validation of Tropical Rainfall Measuring Mission microwave sea surface temperatures, *J. Geophys. Res.*, *109*, C04021, doi:10.1029/2003JC002092.

Gettelman, A., V. P. Walden, L. M. Miloshevich, W. L. Roth, and B. Halter (2006), Relative humidity over Antarctica from radiosondes, satellites, and a general circulation model, *J. Geophys. Res.*, *111*, D09S13, doi:10.1029/2005JD006636.

Jackson, D. L., G. A. Wick, and J. J. Bates (2006), Near-surface retrieval of air temperature and specific humidity using multisensor microwave satellite observations, *J. Geophys. Res.*, *111*, D10306, doi:10.1029/2005JD006431.

Kubota, M., and H. Tomita (2007), Present state of the J-OFURO air-sea interaction data product, *Flux News*, *4*, 13–15.

Kuhlbrodt, T., A. Griesel, M. Montoya, A. Levermann, M. Hofmann, and S. Rahmstorf (2007), On the driving processes of the Atlantic Meridional Overturning Circulation, *Rev. Geophys.*, *45*, RG2001, doi:10.1029/2004RG000166.

Mears, C., D. Smith, and F. J. Wentz (2001), Comparison of SSM/I and buoy-measured wind speeds from 1987–1997, *J. Geophys. Res.*, *106*, 11,719–11,729, doi:10.1029/1999JC000097.

Merchant, C. J., and A. R. Harris (1999), Toward the elimination of bias in satellite retrievals of skin sea surface temperature: 2. Comparison with in situ measurements, *J. Geophys. Res.*, *104*, 23,579–23,590, doi:10.1029/1999JC900106.

Pegion, P. J., M. A. Bourassa, D. M. Legler, and J. J. O'Brien (2000), Objectively derived daily "winds" from satellite scatterometer data, *Mon. Weather Rev.*, *128*, 3150–3168, doi:10.1175/1520-0493(2000)128<3150:ODDWFS>2.0.CO;2.

Singh, R., P. C. Joshi, and C. M. Kishtawal (2005), A new technique for estimation of surface latent heat fluxes using satellite-based observations, *Mon. Weather Rev.*, *133*, 2692–2710, doi:10.1175/MWR2993.1.

Smith, S. D. (1988), Coefficients for sea surface wind stress, heat flux and wind profiles as a function of wind speed and temperature, *J. Geophys. Res.*, *93*, 15,467–15,472, doi:10.1029/JC093iC12p15467.

Sprintall, J. (2003), Seasonal to interannual upper-ocean variability in the Drake Passage, *J. Mar. Res.*, *61*, 1–31, doi:10.1357/002224003321586408.

Susskind, J., C. D. Barnet, and J. M. Blaisdell (2003), Retrieval of atmospheric and surface parameters from AIRS/AMSU/HSB data in the presence of clouds, *IEEE Trans. Geosci. Remote Sens.*, *41*, 390–409, doi:10.1109/TGRS.2002.808236.

Susskind, J. C. Barnet, J. Blaisdell, L. Iredell, F. Keita, L. Kouvaris, G. Molnar, and M. Chahine (2006), Accuracy of geophysical parameters derived from Atmospheric Infrared Sounder/Advanced Microwave Sounding Unit as a function of fractional cloud cover, *J. Geophys. Res.*, *111*, D09S17, doi:10.1029/2005JD006272.

Taylor, P. K. (2000), Intercomparison and validation of ocean-atmosphere energy flux fields, final report of the Joint WCRP/SCOR Working Group on Air-Sea Fluxes, *Rep. WCRP-112*, 306 pp., World Climate Res. Programme, Geneva, Switzerland.

Tobin, D. C., et al. (2006), Atmospheric radiation measurement site atmospheric state best estimates for Atmospheric Infrared Sounder temperature and water vapor retrieval validation, *J. Geophys. Res.*, *111*, D09S14, doi:10.1029/2005JD006103.

Tomita, H., and M. Kubota (2006), An analysis of the accuracy of Japanese Ocean Flux data sets with Use of Remote sensing Observations (J-OFURO) satellite-derived latent heat flux using moored buoy data, *J. Geophys. Res.*, *111*, C07007, doi:10.1029/2005JC003013.

Vazquez-Cuervo, J., E. Armstrong, and A. Harris (2004), The effects of aerosols and clouds on the retrieval of satellite derived infrared sea surface temperatures, *J. Clim.*, *17*, 3921–3933, doi:10.1175/1520-0442(2004)017<3921:TEOAAC>2.0.CO;2.

Wentz, F. J., and T. Meissner (2000), AMSR ocean algorithm, algorithm theoretical basis document, version 2, Remote Sens. Syst., Santa Rosa, Calif.

Wentz, F. J., and T. Meissner (2007), AMSR-E ocean algorithms, *Rep. 051707*, 6 pp., Remote Sens. Syst., Santa Rosa, Calif.

Yu, L., and R. A. Weller (2007), Objectively analyzed air-sea heat fluxes for the global ice-free oceans (1981–2005), *Bull. Am. Meteorol. Soc.*, *88*, 527–539, doi:10.1175/BAMS-88-4-527.

S. Dong (corresponding author), Cooperative Institute for Marine and Atmospheric Studies, Rosenstiel School of Marine and Atmospheric Science, University of Miami, Miami, FL 33149, USA. (shenfu.dong@noaa.gov)

E. J. Fetzer, Jet Propulsion Laboratory, Pasadena, CA 91109, USA.

S. T. Gille and J. Sprintall, Scripps Institution of Oceanography, University of California, San Diego, CA 92037, USA.